The relative effects of the accretionary wedge and sedimentary layer on the rupture process of subduction zone earthquakes

Xian Li[1][2], Yihe Huang[3]

[1]Key Laboratory of Earth and Planetary Physics, Institute of Geology and Geophysics, Chinese Academy of Sciences, Beijing 100029, China.

[2]College of Earth and Planetary Sciences, University of Chinese Academy of Sciences, Beijing 100049, China.

[3]Department of Earth and Environmental Sciences, University of Michigan, Ann Arbor, MI 48109, USA.

Corresponding author: Xian Li (lixian@mail.iggcas.ac.cn)

Key Points:

- Our rupture simulations unveil the relative effects of accretionary wedges and sedimentary layers on earthquake slip and ground motions.

- The two structures can have opposite effects on slip, but their co-existence always enhances fault slip and amplifies ground motions.

- The enhancement effect on fault slip increases with shallower up-dip rupture extent and hence earthquake magnitude.

28 **Abstract**

29

30 Low-velocity accretionary wedges and sedimentary layers overlying continental plates widely

31 exist in subduction zones. However, the two structures are commonly neglected in velocity

32 models used in slip inversion, ground motion estimation, and dynamic rupture simulation, which

33 may cause a biased estimation of coseismic slip and near-fault ground motions during subduction

34 zone earthquakes. We use the 2011 M_w 9.0 Tohoku-Oki earthquake as an example and reproduce

35 the observed seafloor deformation using 2-D dynamic rupture models with or without an

36 accretionary wedge and a sedimentary layer. We find that the co-existence of the accretionary

37 wedge and sedimentary layer significantly enhances the shallow coseismic slip and amplifies

38 ground accelerations near the accretionary wedge. Hence, stress drop on the shallow fault

39 estimated from the coseismic slip or surface deformation is overestimated when the two

40 structures are neglected. We further simulate a suite of earthquakes where the up-dip rupture

41 terminates at different depths. Results show that a sedimentary layer enhances coseismic slip in

42 all cases, while an accretionary wedge can lead to a sharper decline in slip when negative

43 dynamic stress drop exists on the shallow fault. However, a combination of the two structures

44 tends to enhance fault slip, especially when rupture breaks through a trench. Thus, their

45 combined effects are nonlinear and can be larger than the respective contribution of each

46 structure. Our results emphasize that subduction zones featuring a co-existence of an

47 accretionary wedge and a sedimentary layer may have inherently higher earthquake and tsunami

48 hazards.

49

50

51 **Plain Language Summary**

52 The accretionary wedge and sedimentary layer are two low-velocity sediment structures widely

53 existing in subduction zones, which can have a great impact on earthquake processes and ground

54 motions. In the 2011 M_w 9.0 Tohoku-Oki earthquake, rupture propagated to the trench with large

55 fault slip on the shallow fault. Our earthquake simulations reveal that considering both structures

56 in the northern Japan trench significantly enhances shallow fault slip during the 2011 M_w 9.0

57 Tohoku-Oki earthquake. By simulating a suite of earthquake scenarios with different rupture

58 extents, we find that the enhancement effects of an accretionary wedge and a sedimentary layer

2

59   on fault slip are especially pronounced when rupture reaches the trench and yet diminish as the

60   up-dip rupture extent becomes deeper. These structures also significantly amplify and prolong

61   ground motions for both large and small earthquakes. Subduction zones that feature a co-

62   existence of the two structures may have a greater potential to accommodate large earthquakes

63   due to their enhancement effects on fault slip.

64

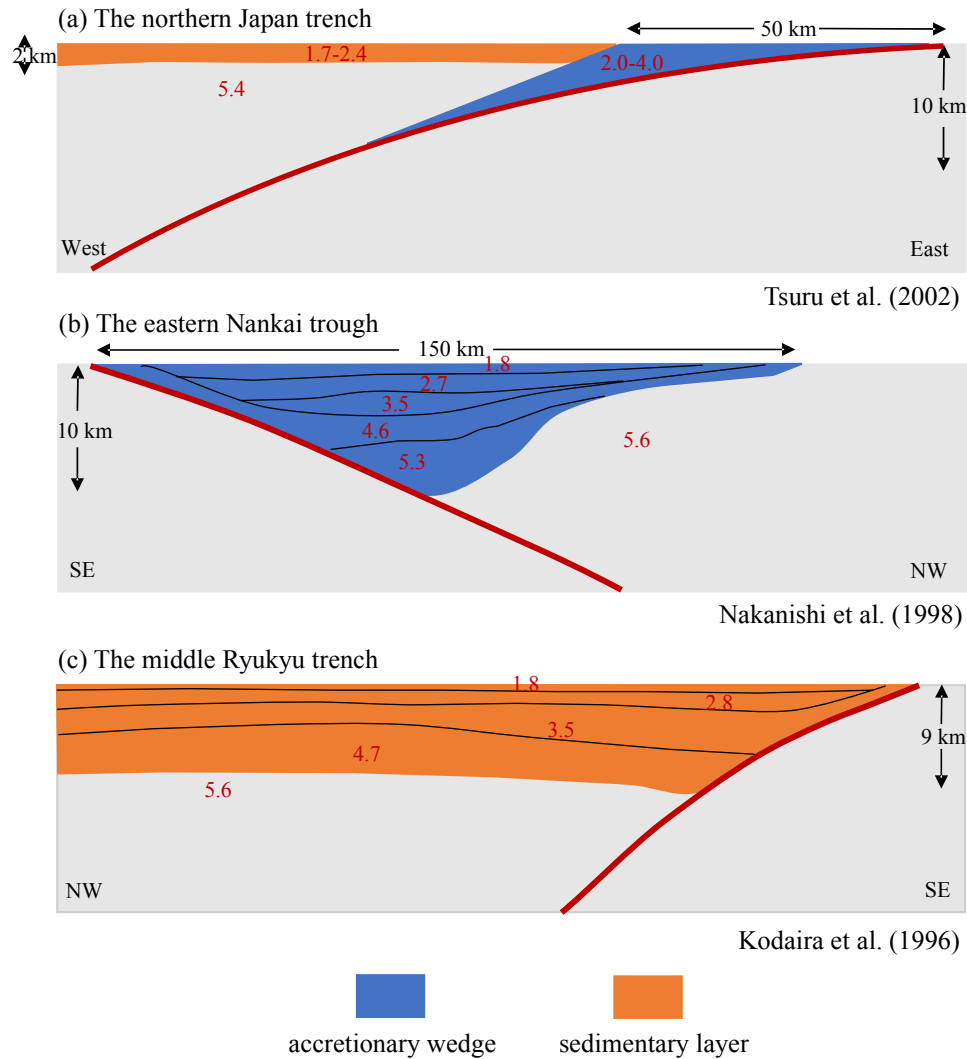65   **1. Introduction**

66

67   Sediments play a key role in the mechanical processes of subduction zones. In the collision

68   margin where an oceanic plate subducts below a continental plate, material offscraped from the

69   downgoing oceanic plate forms a wedge-shaped low-velocity sediment zone called an

70   accretionary wedge. Accretionary wedges are widely observed in subduction zones (Table 1).

71   For example, in the northern Japan trench where the 2011 Tohoku-Oki earthquake occurred, a

72   wedge-shaped sedimentary unit with P-wave velocities of 2.0-4.0 km/s is located at the seaward

73   end of the continental plate and extends to a depth greater than 13 km (Tsuru et al., 2002). The

74   accretionary wedge in the eastern Nankai trough consists of five layers having seismic velocities

75   of 1.8, 1.9-2.7, 2.8-3.5, 3.8-4.6, and 4.6-5.3 km/s (Nakanishi et al., 1998). In the Cascadia

76   subduction zone, the accretionary wedge is wide from Vancouver to northern Oregon but is

77   narrow from southern Oregon to northern California (Gulick et al., 1998). Along the Peru-Chile

78   trench, the size of the frontal accretionary complex is variable, with accreted sediments

79   appearing in the margin of south-central Chile but absenting in Peru (Flueh et al., 1998;

80   Krabbenhöft et al., 2004).

81

82   Besides accretionary wedges, sedimentary layers overlying continental plates are common

83   features in subduction zones, as shown by the map of *Total Sediment Thickness of the World's*

84   *Oceans and Marginal Seas* (Divins, 2003). In Sumatra, north Japan, Aleutians, Cascadia, and

85   central Chile, nearshore deposits accumulated on the continental margins, making up the several

86   kilometers thick sedimentary layers. These sedimentary layers have relatively lower P-wave

87   velocities of 2-3 km/s compared to accretionary wedges, which complicates the lateral material

88   variation (Table 1). Taking the northern Japan trench, eastern Nankai trough, and middle Ryukyu

89   trench as examples, the conceptual diagrams in Figure 1 demonstrate three simplified scenarios

3

about the distribution of sediments on the overriding plate. In the northern Japan trench, both the accretionary wedge and sedimentary layer are observed. The eastern Nankai trough has an accretionary wedge but no sedimentary layer, whereas there are only sedimentary layers in the middle Ryukyu trench.

Table 1. Dimensions and P-wave velocities of accretionary wedges and sedimentary layers in subduction zones

Subduction Zone	Accretionary wedge		Sedimentary layer		Reference
	Width (km)	P-wave velocity (km/s)	Thickness (km)	P-wave velocity (km/s)	
Makran	>100	1.8-4.4	N/A	N/A	Kopp et al., 2000
Sumatra	30	3.0-3.9	3-5	2.0-3.0	Kopp et al., 2001
Ryukyu trench	N/A	N/A	9	1.8-4.7	Kodaira et al., 1996
Nankai trough	150	1.8-5.3	N/A	N/A	Nakanishi et al., 1998
North Japan trench	40-60	2.0-4.0	2	1.7-2.4	Tsuru et al., 2002; Kimura et al., 2012
South Kuril	10	2.4-3.7	1-2	1.9-2.1	Klaeschen et al., 1994
Central Kuril	N/A	N/A	1-2	1.9-2.2	Klaeschen et al., 1994
North Kuril	18	2.4-2.8	1-2	2.0-2.2	Klaeschen et al., 1994
Aleutians	20-30	2.5-4.5	2-3	2.0-3.0	Holbrook et al., 1999
Alaska	30	1.5-4.5	1-2	1.5-2.4	Brocher et al., 1994; von Huene et al., 1998
Cascadia	50-100	4.5-5.0	3-5	2.0-3.0	Gulick et al., 1998; Parsons et al., 1998
Costa Rica	N/A	N/A	2-4	2.2-4.0	Sallarès et al., 2001
Peru	N/A	N/A	1-3	1.7-3.0	Krabbenhöft et al., 2004
Central Chile	35-50	3.0-4.0	1-3	2.0-2.3	Flueh et al., 1998

4

(a) The northern Japan trench

2 km

1.7-2.4

2.0-4.0

50 km

5.4

10 km

West

East

Tsuru et al. (2002)

(b) The eastern Nankai trough

150 km

1.8

2.7

3.5

4.6

5.3

5.6

10 km

SE

NW

Nakanishi et al. (1998)

(c) The middle Ryukyu trench

1.8

2.8

3.5

4.7

5.6

9 km

NW

SE

Kodaira et al. (1996)

accretionary wedge   sedimentary layer

Figure 1. Conceptual diagrams showing sediment distribution on the overriding plate. (a) Co-existence of an accretionary wedge and a sedimentary layer. (b) Existence of an accretionary wedge only. (c) Existence of sedimentary layers only. Bold red curves represent the plate interface. The accretionary wedge is shown in blue, and the sedimentary layer is shown in orange. The numbers denote P-wave velocities (km/s) (Tsuru et al., 2002; Nakanishi et al., 1998; Kodaira et al., 1996).

In the last century, M_w 8.5 and above earthquakes occurred in the Sumatra, north Japan, Kuril, Kamchatka, Aleutians, Alaska, and south-central Chile subduction zones. These subduction zones all feature a co-existence of accretionary wedges and sedimentary layers, which can have a great impact on coseismic slip and ground motions of subduction zone earthquakes in two aspects: 1) The low-velocity materials cause larger strain given the same stress according to Hooke's Law, which means larger coseismic slip at the base of accretionary wedges and larger

5

112 deformation on the surface of sediments; 2) Reflected waves generated within these low-velocity

113 structures can modulate rupture dynamics and induce high-frequency ground motions. Numerical

114 models conducted by Lotto et al. (2017) and Zelst et al. (2019) suggested that more compliant

115 accretionary wedges in subduction zones cause greater shallow slip. Ma and Hirakawa (2013)

116 demonstrated that the Coulomb failure in the overriding wedge tends to give rise to significant

117 seafloor uplift and depletion in the high-frequency radiation in dynamic rupture simulations.

118 Kozdon and Dunhuam (2013) and Murphy et al. (2018) explored dynamic rupture models with

119 depth-dependent material properties to understand rupture processes of megathrust earthquakes.

120 However, these models neglected the top sedimentary layer that has even lower P-wave

121 velocities than accretionary wedges. Although such a layer is thin in some subduction zones

122 (Table 1), it can have a significant impact on rupture processes. Moreover, in subduction zones

123 having both an accretionary wedge and a sedimentary layer, the combined effects of the two

124 structures on earthquake rupture processes and ground motions are yet unclear.

125

126 Here we first use the M_w 9.0 Tohoku-Oki earthquake rupture as an example to understand the

127 role of accretionary wedges and sedimentary layers. We choose this earthquake as its source

128 process is constrained by abundant observations, including seafloor geodetic observations (Kido

129 et al.,2011; Sato et al., 2011), ocean-bottom pressure gauge data (Ito et al., 2011), and multibeam

130 bathymetric data (Fujiwara et al., 2011). Slip inversions based on seismic recordings, geodetic

131 data, tsunami data, and combinations of different data sets supported huge coseismic slip (> 50

132 m) in the shallow region of the plate boundary (Lay, 2018). A number of dynamic rupture

133 models have been proposed for the 2011 Tohoku-Oki earthquake to elucidate the rupture

134 process, and they mainly focused on the effects of fault friction and stress state on slip

135 distribution and rupture propagation (Kato and Yoshida, 2011; Duan, 2012; Mitsui et al., 2012;

136 Huang et al., 2012 and 2014; Noda and Lapusta, 2013; Kozdon and Dunham, 2013; Cubas et al.,

137 2015). However, most slip inversion models and dynamic rupture simulations were based on an

138 elastic homogeneous medium or a 1-D layer model neglecting the low-velocity accretionary

139 wedge and sedimentary layer, which may cause a biased estimation of coseismic slip, stress

140 drop, and ground motions. With both the accretionary wedge and sedimentary layer widely

141 overlying the continental plate in the northern Japan trench (Tsuru et al., 2002), it is instrumental

142 to understand the separate and combined effects of these near-source structures on the large

143 seafloor deformation near the trench during the 2011 Tohoku-Oki earthquake.

144

145 As most seafloor deformation observation in the 2011 Tohoku-Oki earthquake concentrated in a

146 direction perpendicular to the trench, we use a 2-D dynamic model to reproduce the observed

147 deformation of the 2011 Tohoku-Oki earthquake by considering an accretionary wedge (aw) and

148 a thin sedimentary layer (sed) overlying the continental plate (aw-and-sed model) (Figure 1a).

149 Compared to a homogeneous medium, our results show that the co-existence of the accretionary

150 wedge and sedimentary layer greatly enhances the coseismic slip on the shallow fault and

151 amplifies ground accelerations near the accretionary wedge. We also show that stress drop on the

152 shallow fault estimated from the coseismic slip or surface deformation is overestimated when the

153 two structures are neglected. We further explore the effects of an accretionary wedge and a

154 sedimentary layer by simulating a range of earthquakes with different rupture extents. We find

155 that a sedimentary layer always enhances coseismic slip in different earthquake scenarios. While

156 an accretionary wedge may reduce near-trench slip when the shallow fault features negative

157 dynamic stress drop, a combination with sedimentary layers tends to enhance shallow slip

158 instead. The enhancement effects on coseismic slip are especially pronounced when rupture

159 breaks through the trench. As the up-dip rupture is deeper, the two structures have a smaller

160 impact on fault slip but still greatly amplify ground accelerations on the overriding plate. We

161 also discuss how our dynamic rupture models can be applied as reference scenarios to earthquake

162 hazard analysis in global subduction zones where accretionary wedges or sedimentary layers

163 exist.

164

165 **2. Model setup**

166

167 We use a 2-D dynamic rupture model containing the main features of the northern Japan trench

168 to reproduce the observed seafloor deformation of the 2011 Tohoku-Oki earthquake. In order to

169 model the earthquake rupture process as realistically as possible, we apply observation data

170 including seismic profile, geology survey, drilling site to constrain our model parameters (Tsuru

171 et al., 2002; Kimura et al., 2012; Ujiie et al., 2013). To isolate the contributions of the

172 accretionary wedge and sedimentary layer on coseismic slip and ground accelerations, we

7

173   compare the aw-and-sed model to three models that only contain an accretionary wedge (aw-

174   only model), a sedimentary layer (sed-only model), and a homogeneous medium (homogeneous

175   model) with the same friction and stress parameters as the aw-and-sed model. An accretionary

176   wedge is located within 50 km landward from the Japan trench axis on the surface and extends to

177   10 km in depth. A 2-km-thick sedimentary layer overlies the continental plate outside the

178   accretionary wedge (Figure 1a). We use P-wave velocities of 2.0 km/s, 4.0 km/s, 5.4 km/s in the

179   accretionary wedge, sedimentary layer, and surrounding zone respectively, in accordance with

180   the seismic survey in the northern Japan trench (Tsuru et al., 2002). We set the Poisson's ratio to

181   0.25 and the density to 3000 kg/m^3 throughout the whole domain. The top of the model domain

182   is a free surface, and an absorbing boundary is applied to the out-most margin to avoid artificial

183   reflections. A 200-km-wide fault with dip angles gradually changing from 6° at the surface to

184   16° at a depth of 50 km is embedded in an elastic half-space. The hypocenter is located at a depth

185   of 21 km (Chu et al., 2011) where we apply a time-weakening method (Andrews, 1985) to

186   nucleate the earthquake. The dynamic rupture process is solved using SEM2DPACK, a software

187   package simulating wave propagation and dynamic fracture using spectral element method

188   (Ampuero, 2009).

189

190   We apply a linear slip-weakening friction law to the fault plane:

191
$$\begin{cases} \mu_s - \dfrac{\mu_s - \mu_d}{D_c} D & D < D_c \\ \mu_d & D \geq D_c \end{cases} \qquad (1)$$

192   Where μ_s is the static friction coefficient, μ_d is the dynamic friction coefficient, D_c is the critical

193   slip distance, and D is slip. Since the fault beneath the accretionary wedge is a bimaterial

194   interface that can lead to instability and ill-posedness due to normal stress perturbation during

195   rupture propagation (Cochard and Rice, 2000; Rubin and Ampuero, 2007; Ampuero and Ben-

196   Zion, 2008), we regularize the normal stress as follows (Huang et al., 2018):
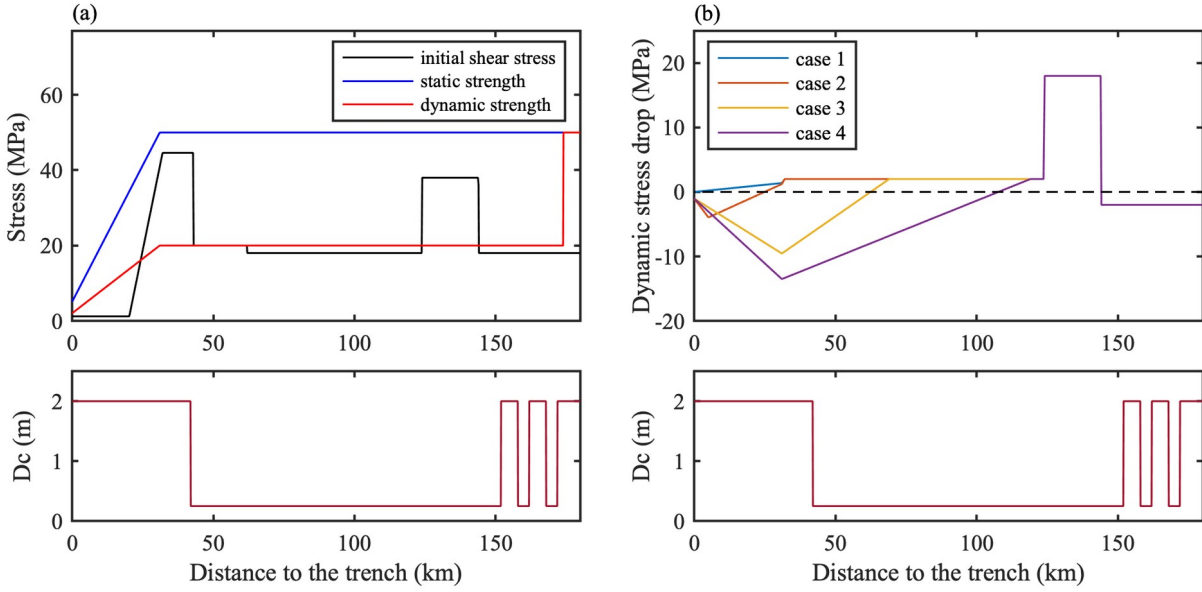
197
$$\frac{d\sigma^\iota}{dt} = \frac{V^\iota}{D_\sigma}\left(\sigma - \sigma^\iota\right) \qquad (2)$$

198   Where σ^ι is the effective normal stress, $V^\iota = 1$ is the reference slip rate, and $D_\sigma = 0.2$ is the

199   reference distance.

200

201   In light of frictional experiments on samples from the Japan Trench Fast Drilling Project (Fulton

202   et al., 2013; Ujiie et al., 2013), we assume a low dynamic friction coefficient and shear stress

203   near the trench. The static and dynamic friction coefficients in our models are 0.5 and 0.2,

204   respectively. The effective normal stress linearly increases from 10 MPa at the surface to a

205   constant value of 100 MPa below 5 km. The static (σ_s) and dynamic shear strengths (σ_d) are

206   calculated by the product between the effective normal stress and the static and dynamic friction

207   coefficients, respectively. The dynamic stress drop ($\Delta\sigma_d$) is the difference between the initial

208   shear stress (τ_0) and dynamic shear strength. In our dynamic models, $\Delta\sigma_d$ is nearly equal to the

209   static stress drop which is the difference between the initial shear stress and the final stress.

210   Positive and negative $\Delta\sigma_d$ represents regions that promote and prohibit rupture propagation,

211   respectively, similar to the velocity-weakening and velocity-strengthening behaviors in rate-and-

212   state friction models. We keep a uniform critical slip distance (D_c) of 2 m at depths above 4 km

213   and 0.25 m around the nucleation zone to facilitate rupture nucleation. We also use small deep

214   asperities with D_c of 0.25 m to reproduce high-frequency radiation of the 2011 Tohoku-Oki

215   earthquake in the down-dip region (Figure 2a) (Huang et al., 2012).

216

217   We determine the initial shear stress τ_0 by fitting the simulated horizontal seafloor deformation

218   of the aw-and-sed model with the observed data. Previous studies presented various types of slip

219   distribution for the 2011 Tohoku-Oki earthquake (Lay, 2018), but most of them revealed large

220   shallow slip. Here we use the slip distribution constrained by the observed seafloor deformation

221   data that includes near-trench locations (Sato et al., 2011; Kido et al., 2011; Ito et al, 2011). It

222   should be noted that the data may have large uncertainties especially for the two points near the

223   trench (~20 m). To reproduce the best-fitting deformation, τ_0 is 38 MPa in the nucleation zone

224   and decreases to 18 MPa in the surrounding region. In the shallow portion of the fault, τ_0

225   increases to 44.6 MPa to fit the large horizontal deformation near the trench, and then linearly

226   decreases to 1.2 MPa and remains constant till the surface (Figure 2a).

227

9

Figure 2. (a) The surface projection of the along-dip distributions of initial shear stress, static strength, dynamic strength (top), and critical slip distance (bottom) for the 2011 Tohoku-Oki earthquake. (b) The surface projection of the along-dip distributions of dynamic stress drop (top) and critical slip distance (bottom) for the four earthquake scenarios in Figure 5.
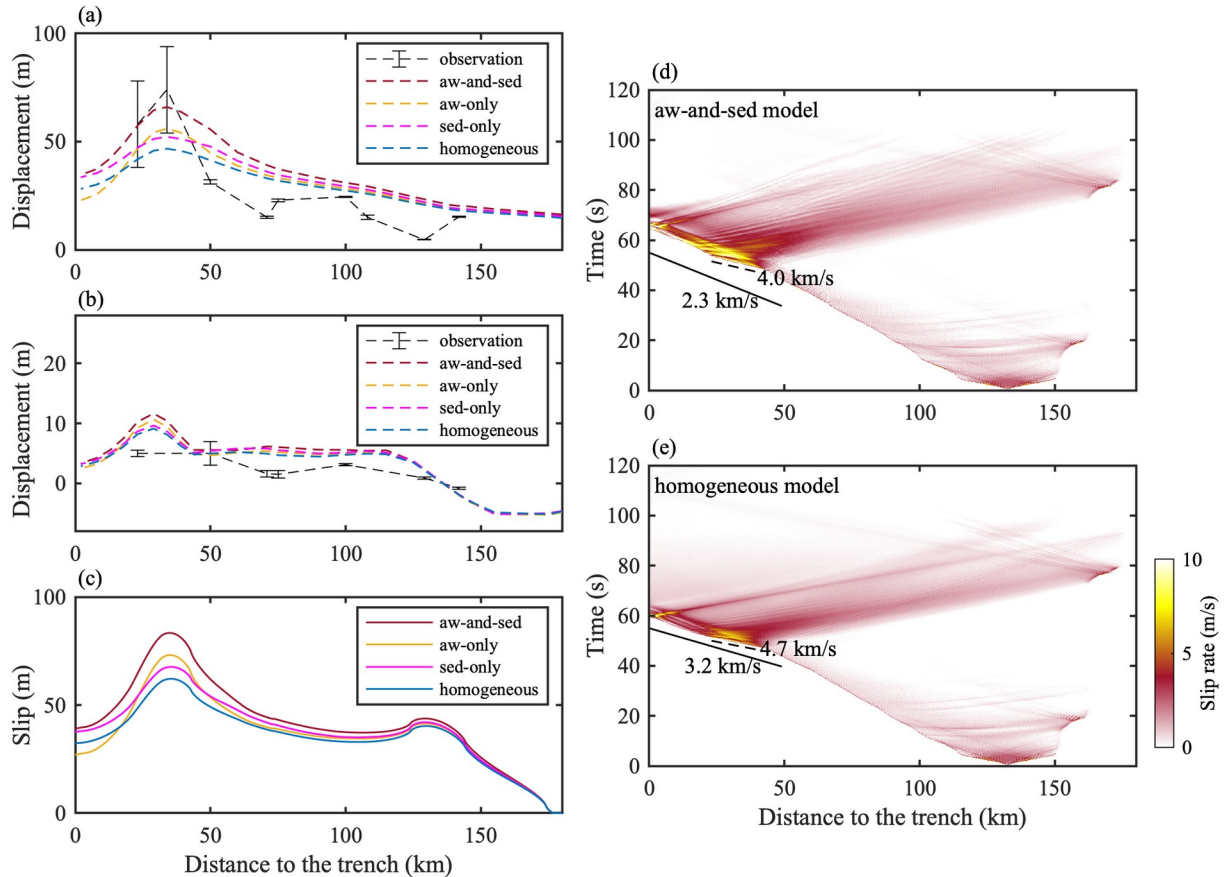
We also simulate a series of earthquake scenarios with up-dip rupture terminating at different depths. We adopt the same model geometry, fault strength, and critical slip distance as the 2011 Tohoku-Oki earthquake but change dynamic stress drop ($\Delta\sigma_d$) on the fault to constrain rupture extents. In particular, we use a shallow region of negative stress drop to prohibit rupture from reaching the trench. Figure 2b shows four earthquake cases of positive $\Delta\sigma_d$ on the entire fault (case 1), negative $\Delta\sigma_d$ at depths above 2.3 km (case 2), 7.7 km (case 3), and 16.5 km (case 4). The same as the 2011 Tohoku-Oki earthquake model, we set $\Delta\sigma_d$ at 18 MPa in the nucleation zone for the four cases.

3. Results

3.1. Slip and rupture dynamics of the 2011 Tohoku-Oki earthquake

The best-fitting aw-and-sed model of the 2011 Tohoku-Oki earthquake explains the large horizontal seafloor deformation at the two near-trench locations (Figure 3a). As the ratio between

10

249   the horizontal and vertical deformation is mainly controlled by the fault-dip angle, the

250   reproduced vertical deformation also has large values near the trench (Figure 3b). In the aw-and-

251   sed model, the coseismic slip increases steeply from a trench-distance of 60 km to 35 km, with a

252   peak slip reaching 83 m, similar to the maximum slip found by Iinuma et al. (2012) by inverting

253   terrestrial GPS observations and seafloor geodetic data. Note that the aw-and-sed model results

254   in slightly larger deformation than the observed deformation at farther distances close to the

255   hypocentral region, due to the dynamic stress drop required for successful nucleation given the

256   frictional parameters used in our model. With the same friction and stress conditions, however,

257   the homogeneous model produces a much flatter slip distribution despite large dynamic stress

258   drop on the shallow fault. Slip in the homogeneous model is lower than that in the aw-and-sed

259   model along the fault, especially in the shallow region, with the peak slip reduced by 25%

260   (Figure 3c). As a result, the largest horizontal and vertical seafloor deformation are reduced by

261   29% and 22%, respectively (Figure 3a and 3b).
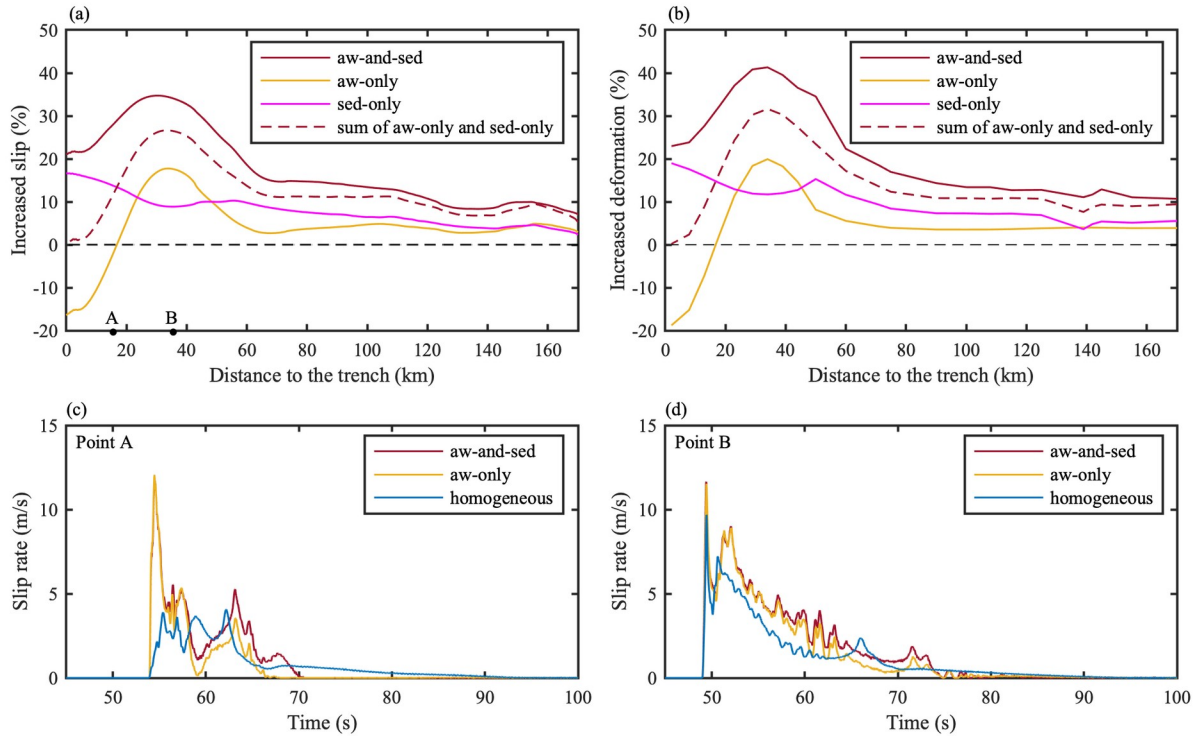
262

263

264   **Figure 3.** Surface deformation, fault slip, and slip rate during the 2011 Tohoku-Oki earthquake. (a)

265   Horizontal surface deformation, (b) vertical surface deformation, and (c) surface projection of fault slip

266   distributions produced by the aw-and-sed, aw-only, sed-only, homogeneous models. Spatiotemporal

267   distributions of slip rate for (d) the aw-and-sed model and (e) the homogeneous model. Black solid lines

268   represent shear wave speeds (2.3 km/s in the accretionary wedge and 3.2 km/s in the homogeneous

269   medium). The black dashed lines represent rupture velocities of 4.0 km/s and 4.7 km/s in the shallow

270   portion of the aw-and-sed model and homogeneous model, respectively.

271

272   We further investigate the respective roles of the accretionary wedge and sedimentary layer on

273   enhancing fault slip and seafloor deformation. Both structures are found to greatly enhance the

274   peak slip and surface deformation during the 2011 Tohoku-Oki earthquake, but the accretionary

275   wedge has a dominant influence. The peak slip of the aw-only and sed-only models is 18% and

276   9% larger than that of the homogeneous model at a trench-distance of 35 km, respectively, while

277   that of the aw-and-sed model is 34% larger at the same location (Figure 3c). The percentage of

278   increased slip in the aw-and-sed model is also larger than the sum of the percentage of increased

279   slip in the aw-only and sed-only models along the fault (Figure 4a). We conclude that the

280   combined effect of the two structures on the coseismic slip of the Tohoku-Oki earthquake is

281   larger than a linear sum of their respective effects, and the same conclusion applies to the

282   horizontal surface deformation (Figure 4b).

283

284   We note that for the aw-only model, fault slip decreases sharply in the shallow region and is

285   smaller than that in a homogeneous medium within a trench-distance of 17 km (Figure 3c). Lotto

286   et al. (2017) found that when accretionary wedges are large and have velocity-strengthening

287   friction at the basement, increasing wedge compliance reduces shallow slip. Our results suggest

288   that the negative dynamic stress drop at the base of accretionary wedges leads to a similar effect,

289   i.e., a more rapid decline in slip and hence a slip reduction compared to a homogeneous medium.

290   However, the results from the sed-only and aw-and-sed models (Figure 4a) indicate that the

291   inclusion of sedimentary layers tends to promote fault slip even when the shallow fault features

292   negative dynamic stress drop. Figures 4c and 4d show the slip rate of the aw-and-sed, aw-only,

293   and homogeneous models at distances of 14 km (point A) and 34 km (point B) from the trench,

294   respectively. Rupture in the aw-only model has larger peak slip rate than in the homogeneous

295   model but shorter rise time at shallow depths (e.g., point A), which leads to smaller slip (Figure

12

296   4c). On the other hand, rupture in the aw-and-sed model features amplified slip rate (Figures 4c

297   and 4d) and prolonged rise time (Figure 4c) compared to the aw-only model, which together

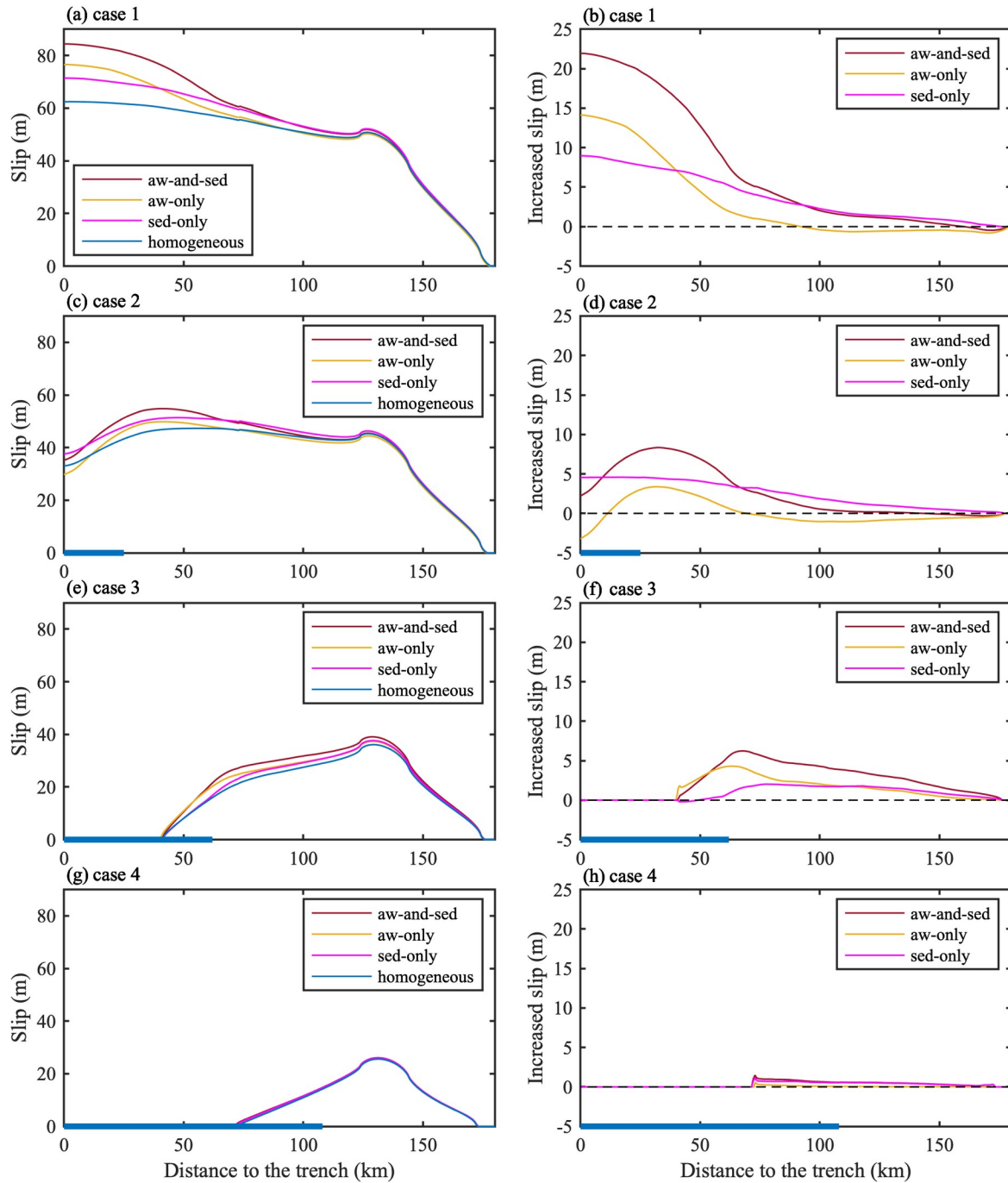298   results in larger slip.

299

300
301   **Figure 4.** Percentage of increased fault slip (a) and surface horizontal deformation (b) in the non-
302   homogeneous models compared with the homogeneous model in the 2011 Tohoku-Oki earthquake. The
303   red dashed lines are the total percentage of the aw-only and sed-only models. (c and d) Slip rate of the
304   aw-and-sed, aw-only, and homogeneous models at points A and B shown in (a), respectively. Note that
305   the slip rate of the three models is regularized to the same start time.
306

307   Besides the effects on fault slip and surface deformation, the accretionary wedge also slows

308   down shallow rupture propagation due to the lower S-wave speed in the accretionary wedge.

309   Rupture propagates at an average speed of 2.5 km/s in the aw-and-sed model in the up-dip

310   direction, compared to a speed of 3.4 km/s in the homogeneous medium. In both models, the

311   shallow asperity with large dynamic stress drop causes local supershear rupture propagation (4

312   km/s in the aw-and-sed model and 4.7 km/s in the homogeneous model) in the up-dip direction

313   (Figure 3d and 3e). Rupture then decelerates to subshear speeds as it propagates to the negative

314   dynamic stress drop region.

13

315

3.2. Earthquake scenarios with different rupture extents

Figure 5. Fault slip and increased slip for earthquakes with rupture extents decreasing from top to

bottom. The left column: comparisons of slip distribution produced by the aw-and-sed, aw-only, sed-only,

and homogeneous models. The right column: increased slip of the three non-homogeneous models in

14

321 comparison to the homogeneous model. Black dashed lines indicate there is no difference between

322 homogeneous and non-homogeneous models. Blue bold lines overlapping with the x-axis denote regions

323 of negative dynamic stress drop.

324

325 In this section, we show that the effects of the accretionary wedge and sedimentary layer on

326 coseismic slip and surface deformation strongly depend on the extent of the shallow rupture,

327 which translates into earthquake magnitude given the same hypocenter location. Figure 5 shows

328 the comparisons of coseismic slip produced by aw-and-sed, aw-only, sed-only, and

329 homogeneous models in four earthquake scenarios when the negative $\Delta\sigma_d$ region extends from

330 surface to depth. The negative $\Delta\sigma_d$ region acts as a barrier prohibiting rupture propagation and

331 thus controls shallow rupture extents. When $\Delta\sigma_d$ is positive on the entire fault, which leads to

332 rupture through the trench, both the accretionary wedge and sedimentary layer greatly enhance

333 fault slip (Figures 5a and 5b). In the case of negative $\Delta\sigma_d$ beneath the outer wedge, rupture

334 reaches the trench but fault slip declines near the trench (Figures 5c and 5d). The accretionary

335 wedge and sedimentary layer greatly enhance the peak slip, but the accretionary wedge leads to a

336 sharper decline in near-trench slip, causing smaller slip than that in the homogeneous model.

337 However, the aw-and-sed model has larger slip on the shallow fault due to the sedimentary layer,

338 which supports the previous finding that the inclusion of sedimentary layers promotes fault slip.

339 As rupture terminates before reaching the trench due to the larger negative $\Delta\sigma_d$ region, the

340 enhancement effects of the accretionary wedge and sedimentary layer on fault slip diminish

341 (Figures 5e and 5f). For the case when rupture does not reach the bottom of the accretionary

342 wedge, the sedimentary layer slightly enhances fault slip and the accretionary wedge has almost

343 no influence (Figures 5g and 5h).

344

345 In conclusion, a sedimentary layer always has a positive effect on the coseismic slip in the four

346 earthquake scenarios, while an accretionary wedge may cause smaller near-trench slip when the

347 dynamic stress drop is negative on the shallow fault. However, a combination of the two

348 structures tends to enhance coseismic slip. The combined effect is significant when rupture

349 reaches the trench and diminishes as the up-dip rupture terminates at deeper depth.
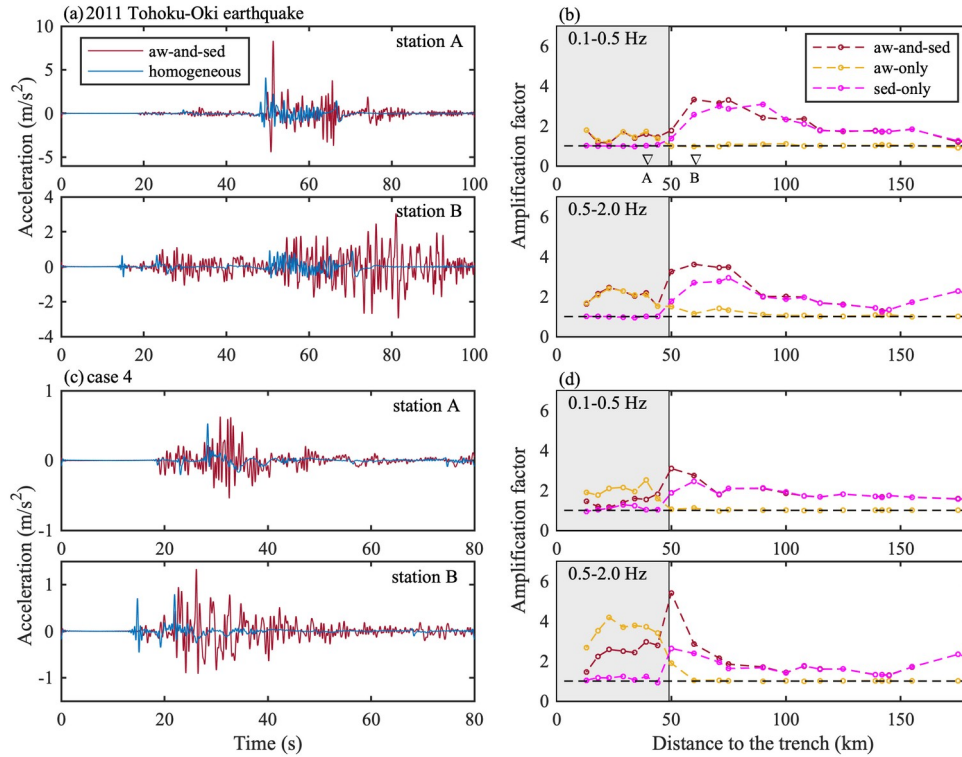
350

351 **3.3. Effects of the accretionary wedge and sedimentary layer on ground accelerations**

15

352

353 We find that the co-existence of the accretionary wedge and sedimentary layer prolongs ground

354 acceleration durations and amplifies peak ground accelerations, but the combined effect behaves

355 differently depending on the shallow rupture extents of earthquakes. In the case of the 2011

356 Tohoku-Oki earthquake, the ground acceleration durations in the aw-and-sed model are

357 significantly prolonged as shown in the accelerograms recorded at two stations inside and

358 outside the accretionary wedge (Figure 6a). Guo et al. (2016) and Kaneko et al. (2019) suggested

359 that accretionary wedges can lead to longer durations of long-period ground motions, due to the

360 surface waves generated from the seaward edge of accretionary wedges or the reverberations of

361 seismic waves within accretionary wedges. To quantify the ground acceleration amplification,

362 the amplification factor is defined as a ratio of peak ground accelerations between non-

363 homogeneous and homogeneous models. We calculate the average amplification factors in two

364 frequency ranges: 0.1-0.5 Hz, 0.5-2.0 Hz. We find that for all stations on the overriding plate, the

365 ground accelerations of the aw-and-sed model are significantly amplified at both 0.1-0.5 Hz and

366 0.5-2.0 Hz (Figure 6b). The maximum amplification effects for both frequency ranges happen in

367 the vicinity of the accretionary wedge. Inside the accretionary wedge, the amplification effect on

368 the ground acceleration at 0.5-2.0 Hz is larger than at 0.1-0.5 Hz (Figure 6b).

369

370

Figure 6. (a) Comparisons of horizontal accelerograms between the aw-and-sed and homogeneous

models; (b) Averaged amplification factors for horizontal ground accelerations at 0.1-0.5 Hz and 0.5-2.0

Hz produced by the three non-homogeneous models during the 2011 Tohoku-Oki earthquake. The

shaded zone is the region inside the accretionary wedge. Black dashed lines represent a value of 1. A

and B are stations located inside and outside the accretionary wedge, respectively. (c) and (d) have the

same representation as (a) and (b), respectively, but for the smaller earthquake in Figure 5g.

377

When rupture does not reach the bottom of the accretionary wedge (case 4 in Figures 5g and 5h),

the two structures can greatly enhance ground accelerations, though they have a minimal

influence on fault slip. However, the combined effect on the ground acceleration amplification is

not always larger than the respective effects. Similar to the 2011 Tohoku-Oki earthquake, the

aw-and-sed model produces longer durations at stations inside and outside the accretionary

wedge (Figure 6c). In the aw-and-sed model, the maximum amplification effects on the ground

accelerations at 0.1-0.5 Hz and 0.5-2.0 Hz are located at the landward edge of the accretionary

wedge where the combined effect of the accretionary wedge and the sedimentary layer is

significantly greater than their linear sum (Figure 6d bottom). Similar to the 2011 Tohoku-Oki

earthquake, the amplification effect inside the accretionary wedge exhibits distinct frequency-

dependence with ground accelerations at 0.5-2.0 Hz in the aw-and-sed and aw-only models being

17

389   more amplified than those at 0.1-0.5 Hz (Figure 6d). These results suggest that dynamic wave

390   interaction inside an accretionary wedge can cause more ground acceleration amplification at

391   high frequencies. The frequency-dependent effect was also observed in the 2016 southeast off-

392   Mie earthquake. Kubo et al. (2019) found that the offshore acceleration response spectra at

393   periods of 0.5-8 s largely exceeds values obtained from the empirical attenuation relationship

394   while that at shorter periods of 0.12 and 0.25 s follows the empirical relationship. The results

395   were interpreted as a large site amplification effect due to an accretionary wedge.

396

397   We notice that for all the stations inside the accretionary wedge, the amplification factors of the

398   aw-and-sed model are obviously smaller than those of the aw-only model, with the ground

399   accelerations at 0.5-2.0 Hz being greatly suppressed in particular (Figure 6d bottom). Thus, for

400   earthquake rupture that does not reach the accretionary wedge, the existence of a sedimentary

401   layer may weaken the amplification effect of the accretionary wedge on ground accelerations

402   inside the accretionary wedge, which may be attributed to wave interference between the two

403   structures.

404

405   **4. Discussion**

406

407   **4.1. Implications for stress drop estimation of the 2011 Tohoku-Oki earthquake**

408

409   Stress release and accumulation on faults are essential to assess regional earthquake hazards. As

410   an important parameter in controlling the source mechanism, stress drop during the 2011

411   Tohoku-Oki earthquake has been investigated by different methods. These studies consider a

412   homogeneous medium, a 1-D layered medium without sedimentary layers, or a 1-D layered

413   medium with sedimentary layers. Brown et al. (2015) estimated a mean stress drop of 2.3 ± 1.3

414   MPa and a peak value of 40 MPa from 40 rupture models of the 2011 Tohoku-Oki earthquake

415   assuming a uniform rigidity of 40 GPa. Assuming a 1-D model without sediment structures, Xie

416   and Cai (2018) constrained an average stress drop of 6.3 MPa from stress inversion of the

417   observed coseismic deformation. Koketsu et al. (2011) calculated an average stress drop of 4.8

418   MPa from the source model constructed through joint inversion of teleseismic, strong motion,

419   and geodetic datasets with sedimentary layers considered in velocity structure.

18

420

421   Here our best-fitting aw-and-sed model reveals a maximum stress drop of 25 MPa on the shallow

422   asperity in the 2011 Tohoku-Oki earthquake (Figure S1). However, to reproduce the same

423   observed peak deformation near the trench, the maximum stress drop on the shallow asperity is

424   ~27 MPa, 27MPa, and 30 MPa for the aw-only, sed-only, and homogeneous models, respectively

425   (Figure S1). This indicates that stress drop on the shallow fault evaluated from fault slip or

426   surface deformation can be overestimated by 20% when accretionary wedge and sedimentary

427   layer are not considered, as the co-existence of the two structures greatly enhances the coseismic

428   slip during the 2011 Tohoku-Oki earthquake. We also calculate the average stress drop from

429   different models using integrated stress drop divided by the rupture length. The average stress

430   drop in the aw-and-sed, aw-only, sed-only, and homogeneous models is 2.5 MPa, 2.7 MPa, 2.8

431   MPa, and 3.2MPa, respectively. The average stress drop in the homogeneous model is 28%

432   larger than that in the aw-and-sed model. Our results suggest that for other large megathrust

433   earthquakes that reach the accretionary wedge, both average and maximum stress drop estimated

434   for a homogeneous medium may be overestimated.

435

436   **4.2. Implications for global megathrust earthquakes**

437

438   In the last century, besides the northern Japan trench, M_w 8.5 and above earthquakes also

439   occurred in the Aleutians, Alaska, Kuril, Kamchatka, south-central Chile, and Sumatra

440   subduction zones. These subduction zones all feature a co-existence of accretionary wedges and

441   sedimentary layers. The two structures could be important factors in controlling large subduction

442   zone earthquakes. Wells et al. (2003) illustrated that rupture zones of great subduction zone

443   earthquakes tend to underlie the forearc basins. Most seaward part of an accretionary wedge

444   exhibits a velocity-strengthening behavior, which is generally thought to impede up-dip rupture

445   (Wang & Hu, 2006). Ma and Nie (2019) showed that coseismic yielding of plentiful sediments in

446   the northern Japan trench margin can induce large inelastic uplift and diminish slip near the

447   trench. However, Gulick et al. (2011) suggested that accreted sediments near the Sunda trench

448   were dewatered and compacted, which allowed a velocity-weakening behavior and hence

449   facilitated the rupture of the 2004 M_w 9.2 Sumatra-Andaman earthquake to the trench. Lotto et al.

19

450   (2017) pointed out that more compliant accretionary wedges in most cases cause greater shallow

451   fault slip, but larger accretionary wedges with velocity-strengthening friction reduce slip.

452

453   Our results indicate that accretionary wedges and sedimentary layers greatly enhance coseismic

454   slip for earthquakes that propagate to trenches or terminate at shallow depths, allowing

455   subduction zones to have a greater potential to accommodate large earthquakes. In the 2004 M_w

456   9.2 Sumatra-Andaman earthquake, the coseismic rupture occurred largely beneath the

457   accretionary wedge in the southern part of the rupture area (Gulick et al., 2011). The upper

458   bound of the coseismic slip during the 2010 M_w 8.8 Chile earthquake reached the toe of the

459   accretionary wedge with peak slips near the trench (Yue et al., 2014). The up-dip limit of the

460   1960 M_w 9.5 great Chile earthquake extends further seaward (Contreras−Reyes et al., 2010). The

461   accretionary wedges and sedimentary layers may have played important roles in enhancing the

462   shallow slip during these large earthquakes. Besides, a co-existence of accretionary wedges and

463   sedimentary layers significantly prolongs and amplifies ground motions near the accretionary

464   wedge (Figure 6), which may induce submarine landslide failure. In Cascadia where great

465   earthquakes are the most likely to occur in the Pacific Northwest United States, ground motion

466   intensity in a future megathrust earthquake was predicted based on kinematic rupture models that

467   do not account for the dynamic effects of low-velocity near-fault structures (Wirth et al., 2018).

468   With wide accretionary wedges and sedimentary layers covering the continental plate (Gulick et

469   al., 1998; Parsons et al., 1998), our results suggest that evaluations of Cascadia seismic hazards

470   should consider the possibility of longer and larger ground motions produced by the two

471   structures as well.

472

473   **4.3. Limitations and future works**

474

475   Since our focus is to evaluate the influence of accretionary wedges and sedimentary layers on the

476   along-dip rupture process, 2-D models that do not account for along-strike variations are used in

477   this work. In the rupture zone of the 2011 Tohoku-Oki earthquake, the wedge-shaped sediments

478   appear in the northern area of the epicenter with dimensions varying along the Japan trench, but

479   in the southern area, the sediments extend in the down-dip direction as a channel-like unit (Tsuru

480   et al., 2002). Future numerical models should be directed towards 3-D rupture simulations to

20

481 address the influence of along-strike heterogeneity on rupture features. On the other hand, we

482 analyze the effects of the accretionary wedge and sedimentary layer on coseismic slip and

483 ground motions assuming purely elastic properties. However, the nature of an accretionary

484 wedge or a sedimentary layer can have viscoelastic and plastic behaviors, which may diminish

485 slip and reduce surface deformation (Ma & Nie, 2019). Since the effect of sedimentary structures

486 should be a combination of elastic and inelastic effects, whether it promotes fault slip also

487 depends on which behavior is in a dominant role. A more realistic approximation of accretionary

488 wedges and sedimentary layers in future works is to incorporate viscoelasticity and plasticity.

489

490 **5. Conclusions**

491

492 Our dynamic rupture simulations of the 2011 Tohoku-Oki earthquake show that the co-existence

493 of the accretionary wedge and sedimentary layer significantly enhances coseismic slip in the

494 shallow region and greatly amplifies ground accelerations near the accretionary wedge. When

495 the shallow fault features negative stress drop, an accretionary may cause smaller near-trench

496 slip, while a combination with a sedimentary layer tends to enhance fault slip. The enhancement

497 effects of the two structures are pronounced when rupture reaches the trench and diminish as the

498 up-dip rupture is deeper. When earthquake rupture does not reach accretionary wedges, a

499 sedimentary layer has a slight enhancement effect on the coseismic slip while an accretionary

500 wedge has almost no influence. But a co-existence of the two structures can greatly amplify

501 ground accelerations on the overriding plate. We suggest that for large megathrust earthquakes

502 that reach shallow fault, stress drop estimated from coseismic slip or surface deformation can be

503 overestimated when accretionary wedges and sedimentary layers are neglected. Our 2-D

504 dynamic rupture models provide a fundamental understanding of how the low-velocity near-fault

505 structures can impact subduction zone earthquake processes and highlight the importance of

506 considering the effects of accretionary wedges and sedimentary layers in seismic observations

507 and numerical modeling of subduction zone earthquakes.

508

509 **Data Availability Statement**

510

21

511 We used Trelis (https://coreform.com/products/trelisnew/) to mesh the geometrical model. The

512 numerical simulations were solved using SEM2DPACK version 2.3.8

513 (http://www.sourceforge.net/projects/sem2d/), and simulation results were visualized by Matlab.

514 The input files to reproduce simulation results and the scripts to plot figures in this paper are

515 available on UM Deep Blue (https://doi.org/10.7302/rerb-bd58).

516

525 **References**

526

527 Ampuero, J. P. (2009). SEM2DPACK: A spectral element method tool for 2D wave propagation

528   and earthquake source dynamics, User's Guide, version 2.3.6. Retrieved from

529   http://www.sourceforge.net/projects/sem2d/

530 Ampuero, J.-P., & Ben-Zion, Y. (2008). Cracks, pulses and macroscopic asymmetry of dynamic

531   rupture on a biomaterial interface with velocity- weakening friction. *Geophysical Journal*

532   *International,* 173(2), 674–692. https://doi.org/10.1111/j.1365-246X.2008.03736.x

533 Andrews, D. J. (1985). Dynamic plane−strain shear rupture with a slip−weakening friction law

534   calculated by a boundary integral method. *Bulletin of the Seismological Society of America,*

535   75(1), 1-21.

536 Brocher, T. M., Fuis, G. S., Fisher, M. A., Plafker, G., Moses, M. J., Taber, J. J., & Christensen,

537   N. I. (1994). Mapping the megathrust beneath the northern Gulf of Alaska using wide-angle

538   seismic data. *Journal of Geophysical Research,* 99(B6), 11663-11685.

539   https://doi.org/10.1029/94JB00111

540 Brown, L., Wang, K., & Sun, T. (2015). Static stress drop in the Mw 9 Tohoku‒oki earthquake:

541   Heterogeneous distribution and low average value. *Geophysical Research Letters,* 42,

542   10595-10600. https://doi.org/10.1002/2015GL066361

543 Chu, R., Wei, S., Helmberger, D. V., Zhan, Z., Zhu, L., &Kanamori, H. (2011). Initiation of the

544   great Mw 9.0 Tohoku-Oki earthquake. *Earth and Planetary Science Letters,* 308, 277-283.

545   https://doi.org/10.1016/j.epsl.2011.06.031

546 Cochard, A., & Rice, J. R. (2000). Fault rupture between dissimilar materials: Ill-posedness,

547   regularization, and slip-pulse response. *Journal of Geophysical Research,* 105(B11),

548   25,891–25,907. https://doi.org/10.1029/2000JB900230

549 Contreras‒Reyes, E., Flueh, E. R., & Grevemeyer, I. (2010). Tectonic control on sediment

550   accretion and subduction off south central Chile: Implications for coseismic rupture

551   processes of the 1960 and 2010 megathrust earthquakes. *Tectonics,* 29, TC6018.

552   https://doi.org/10.1029/2010TC002734

553 Cubas, N., Lapusta, N., Avouac, J.-P., & Perfettini, H. (2015). Numerical modeling of long-term

554   earthquake sequences on the NE Japan megathrust: Comparison with observations and

555   implications for fault friction. *Earth and Planetary Science Letters,* 419, 187-198.

556   https://doi.org/10.1016/j.epsl.2015.03.002

557 Divins, D. (2003). *Total Sediment Thickness of the World's Oceans & Marginal Seas.* Boulder,

558   CO: NOAA National Geophysical Data Center.

559 Duan, B. (2012). Dynamic rupture of the 2011 Mw 9.0 Tohoku-Oki earthquake: Roles of a

560   possible subducting seamount. *Journal of Geophysical Research,* 117, B05311.

561   https://doi.org/10.1029/2011JB009124

562 Flueh, E. R., Vidal N., Ranero, C. R., Hojka, A., von Huene, R., Bialas, J., et al. (1998). Seismic

563   investigation of the continental margin off‒ and onshore Valparaiso, Chile. *Tectonophysics,*

564   288, 251–263.

565 Fujiwara, T., Kodaira, S., No, T., Kaiho, Y., Takahashi, N., & Kaneda, Y. (2011). The 2011

566   Tohoku-Oki earthquake: Displacement reaching the trench axis. *Science,* 334, 1240. https://

567   doi.org/10.1126/science.1211554

568 Fulton, P., Brodsky, E., Kano, Y., Mori, J., Chester, F., Ishikawa, T., et al. (2013). Low

569   coseismic friction on the Tohoku-Oki fault determined from temperature measurements.

570   *Science,* 342, 1214-1217. https://doi.org/10.1126/science.1243641

571 Gulick, S. P. S., Austin, J. A., McNeill, L. C., Bangs, N. L. B., Martin, K. M., Henstock, T. J., et
572   al. (2011). Updip rupture of the 2004 Sumatra earthquake extended by thick indurated
573   sediments. *Nature Geoscience,* 4, 453-456. https://doi.org/10.1038/ngeo1176

574 Gulick, S. P. S., Meltzer, A. M., & Clarke, S. H. (1998). Seismic structure of the southern
575   Cascadia subduction zone and accretionary prism north of the Mendocino triple junction.
576   *Journal of Geophysical Research,* 103(B11), 27207-27222.
577   https://doi.org/10.1029/98JB02526

578 Guo, Y., Koketsu, K., & Miyake, H. (2016). Propagation mechanism of long-period ground
579   motions for offshore earthquakes along the Nankai trough: Effects of the accretionary
580   wedge. *Bulletin of the Seismological Society of America,* 106(3), 1176-1197. https://doi.org/
581   10.1785/0120150315

582 Holbrook, W. S., Lizarralde, D., McGeary, S., Bangs, N., & Diebold, J. (1999). Structure and
583   composition of the Aleutian island arc and implications for continental crustal growth.
584   *Geology,* 27(1), 31-34. https://doi.org/10.1130/0091-
585   7613(1999)027<0031:SACOTA>2.3.CO;2

586 Huang, Y. (2018). Earthquake rupture in fault zones with along−strike material heterogeneity.
587   *Journal of Geophysical Research: Solid Earth,* 123, 9884-9898.
588   https://doi.org/10.1029/2018JB016354

589 Huang, Y., Ampuero, J.-P., & Kanamori, H. (2014). Slip-weakening models of the 2011
590   Tohoku-Oki earthquake and constraints on stress drop and fracture energy. *Pure and*
591   *Applied Geophysics,* 171, 2555-2568. https://doi.org/10.1007/s00024-013-0718-2

592 Huang, Y., Meng, L., & Ampuero, J.-P. (2012). A dynamic model of the frequency-dependent
593   rupture process of the 2011 Tohoku-Oki earthquake. *Earth, Planets and Space,* 64, 1061-
594   1066. https://doi.org/10.5047/eps.2012.05.011

595 Iinuma, T., Hino, R., Kido, M., Inazu, D., Osada, Y., Ito, Y., et al. (2012). Coseismic slip
596   distribution of the 2011 off the Pacific Coast of Tohoku Earthquake (M9.0) refined by
597   means of seafloor geodetic data. *Journal of Geophysical Research,* 117, B07409.
598   https://doi.org/10.1029/2012JB009186

599 Ito, Y., Tsuji, T., Osada, Y., Kido, M., Inazu, D., Hayashi, Y., et al. (2011). Frontal wedge
600   deformation near the source region of the 2011 Tohoku-Oki earthquake. *Geophysical*
601   *Research Letters,* 38, L00G05. https://doi.org/10.1029/2011GL048355

602   Kaneko, Y., Ito, Y., Chow, B., Wallace, L. M., Tape, C., Grapenthin, R., et al. (2019). Ultralong
603   duration of seismic ground motion arising from a thick, low−velocity sedimentary wedge.
604   *Journal of Geophysical Research: Solid Earth,* 124, 10347-10359.
605   https://doi.org/10.1029/2019JB017795

606   Kato, N., & Yoshida, S. (2011). A shallow strong patch model for the 2011 great Tohoku−oki
607   earthquake: A numerical simulation. *Geophysical Research Letters,* 38, L00G04.
608   https://doi.org/10.1029/2011GL048565

609   Kido, M., Osada, Y., Fujimoto, H., Hino, R., & Ito, Y. (2011). Trench-normal variation in
610   observed seafloor displacements associated with the 2011 Tohoku-Oki earthquake.
611   *Geophysical Research Letters,* 38, L24303. https://doi.org/10.1029/2011GL050057

612   Kimura, G., Hina, S., Hamada, Y., Kameda, J., Tsuji, T., Kinoshita, M., & Yamaguchi, A.
613   (2012). Runaway slip to the trench due to rupture of highly pressurized megathrust beneath
614   the middle trench slope: The tsunamigenesis of the 2011 Tohoku earthquake off the east
615   coast of northern Japan. *Earth and Planetary Science Letters,* 339-340, 32-45.
616   https://doi.org/10.1016/j.epsl.2012.04.002

617   Klaeschen, D., Belykh, I., Gnibidenko, H., Patrikeyev, S., & von Huene, R. (1994). Structure of
618   the Kuril Trench from seismic reflection records. *Journal of Geophysical Research,*
619   99(B12), 24173-24188. https://doi.org/10.1029/94JB01186

620   Kodaira, S., Iwasaki, T., Urabe, T., Kanazawa, T., Egloff, F., Makris, J., & Shimamura, H.
621   (1996). Crustal structure across the middle Ryukyu trench obtained from ocean bottom
622   seismographic data. *Tectonophysics,* 263, 39-60. https://doi.org/10.1016/S0040-
623   1951(96)00025-X

624   Koketsu, K., Yokota, Y., Nishimura, N., Yagi, Y., Miyazaki, S., Satake, K., et al. (2011). A
625   unified source model for the 2011 Tohoku earthquake. *Earth and Planetary Science Letters,*
626   310, 480-487. https://doi.org/10.1016/j.epsl.2011.09.009

627   Kopp, C., Fruehn, J., Flueh, E. R., Reichert, C., Kukowski, N., Bialas, J., & Klaeschen, D.
628   (2000). Structure of the makran subduction zone from wide-angle and reflection seismic
629   data. *Tectonophysics,* 329, 171-191. https://doi.org/10.1016/S0040-1951(00)00195-5

630   Kopp, H., Flueh, E. R., Klaeschen, D., Bialas, J., & Reichert, C. (2001). Crustal structure of the
631   Central Sunda margin at the onset of oblique subduction. *Geophysical Journal*
632   *International,* 147, 449-474. https://doi.org/10.1046/j.0956-540X.2001.01547.x

633   Kozdon, J. E., & Dunham, E. M. (2013). Rupture to the Trench: Dynamic rupture simulations of
634   the 11 March 2011 Tohoku earthquake. *Bulletin of the Seismological Society of America,*
635   103(2B), 1275-1289. https://doi.org/10.1785/0120120136

636   Krabbenhöft, A., Bialas, J., Kopp, H., Kukowski, N., & Hübscher, C. (2004). Crustal structure of
637   the Peruvian continental margin from wide-angle seismic studies. *Geophysical Journal*
638   *International,* 159, 749-764. https://doi.org/10.1111/j.1365-246X.2004.02425.x

639   Kubo, H., Nakamura, T., Suzuki, W., Dhakal, Y. P., Kimura, T., Kunugi, T., et al. (2019).
640   Ground-motion characteristics and nonlinear soil response observed by donet1 seafloor
641   observation network during the 2016 southeast off-Mie, Japan, Earthquake. *Bulletin of the*
642   *Seismological Society of America,* 109(3), 976-986. https://doi.org/10.1785/0120170296

643   Lay, T. (2018). A review of the rupture characteristics of the 2011 Tohoku-oki Mw 9.1
644   earthquake. *Tectonophysics,* 733, 4-36. https://doi.org/10.1016/j.tecto.2017.09.022

645   Lotto, G. C., Dunham, E. M., Jeppson, T. N., & Tobin, H. J. (2017). The effect of compliant
646   prisms on subduction zone earthquakes and tsunamis. *Earth and Planetary Science Letters,*
647   458, 213-222. https://doi.org/10.1016/j.epsl.2016.10.050

648   Ma, S., & Hirakawa, E. T. (2013). Dynamic wedge failure reveals anomalous energy radiation of
649   shallow subduction earthquakes. *Earth and Planetary Science Letters,* 375, 113-122. https://
650   doi.org/10.1016/j.epsl.2013.05.016

651   Ma, S., & Nie, S. (2019). Dynamic Wedge Failure and Along-Arc Variations of Tsunamigenesis
652   in the Japan Trench Margin. *Geophysical Research Letters,* 46, 8782-8790.
653   https://doi.org/10.1029/2019GL083148

654   Mitsui, Y., Kato, N., Fukahata, Y., & Hirahara, K. (2012). Megaquake cycle at the Tohoku
655   subduction zone with thermal fluid pressurization near the surface. *Earth and Planetary*
656   *Science Letters,* 325-326, 21-26. https://doi.org/10.1016/j.epsl.2012.01.026

657   Murphy, S., Di Toro, G., Romano, F., Scala, A., Lorito, S., Spagnuolo, E., et al. (2018).
658   Tsunamigenic earthquake simulations using experimentally derived friction laws. *Earth and*
659   *Planetary Science Letters,* 486, 155–165. https://doi.org/10.1016/j.epsl.2018.01.011

660   Nakanishi, A., Shiobara, H., Hino, R., Kodaira, S., Kanazawa, T., & Shimamura, H. (1998).
661   Detailed subduction structure across the eastern Nankai Trough obtained from ocean bottom
662   seismographic profiles. *Journal of Geophysical Research,* 103(B11), 27151-27168.
663   https://doi.org/10.1029/98JB02344

664 Noda, H., & Lapusta, N. (2013). Stable creeping fault segments can become destructive as a
665   result of dynamic weakening. *Nature,* 493, 518-521. https://doi.org/10.1038/nature11703

666 Parsons, T., Trehu, A. M., Luetgert, J. H., Miller, K., Kilbride, F., Wells, R. E., et al. (1998). A
667   new view into the Cascadia subduction zone and volcanic arc: Implications for earthquake
668   hazards along the Washington margin. *Geology,* 26(3), 199-202.
669   https://doi.org/10.1130/0091-7613(1998)026<0199:ANVITC>2.3.CO;2

670 Rubin, A. M., & Ampuero, J.-P. (2007). Aftershock asymmetry on a biomaterial interface.
671   *Journal of Geophysical Research,* 112, B05307. https://doi.org/10.1029/2006JB004337

672 Sallarès, V., Dañobeitia, J. J., & Flueh, E. R. (2001). Lithospheric structure of the Costa Rican
673   Isthmus: Effects of subduction zone magmatism on an oceanic plateau. *Journal of*
674   *Geophysical Research,* 106(B1), 621-643. https://doi.org/10.1029/2000JB900245

675 Sato, M., Ishikawa, T., Ujihara, N., Yoshida, S., Fujita, M., Mochizuki, M., & Asada, A. (2011).
676   Displacement above the hypocenter of the 2011 Tohoku-Oki earthquake. *Science,* 332,
677   1395. https://doi.org/10.1126/science.1207401

678 Tsuru, T., Park, J.-O., Miura, S., Kodaira, S., Kido, Y., & Hayashi, T. (2002). Along-arc
679   structural variation of the plate boundary at the Japan Trench margin: Implication of
680   interplate coupling. *Journal of Geophysical Research,* 107(B12), 2357.
681   https://doi.org/10.1029/2001jb001664

682 Ujiie, K., Tanaka, H., Saito, T., Tsutsumi, A., Mori, J., & Toczko, S. (2013). Low coseismic
683   shear stress on the Tohoku-Oki megathrust determined from laboratory experiments.
684   *Science,* 342, 1211-1214. DOI: 10.1126/science.1243485

685 van Zelst, I., Wollherr, S., Gabriel, A.-A., Madden, E. H., & van Dinther, Y. (2019). Modeling
686   megathrust earthquakes across scales: one-way coupling from geodynamics and seismic
687   cycles to dynamic rupture. *Journal of Geophysical Research: Solid Earth,* 124, 11414–
688   11446. https://doi.org/10.1029/ 2019JB017539

689 von Huene, R., Klaeschen, D., Gutscher, M., & Fruehn, J. (1998). Mass and fluid flux during
690   accretion at the Alaskan margin. *The Geological Society of America Bulletin,* 110(4), 468-
691   482. https://doi.org/10.1130/0016-7606(1998)110<0468:MAFFDA>2.3.CO;2

692 Wang, K., & Hu, Y. (2006). Accretionary prisms in subduction earthquake cycles: The theory of
693   dynamic Coulomb wedge. *Journal of Geophysical Research,* 111, B06410.
694   https://doi.org/10.1029/2005JB004094

695 Wells, R. E., Blakely, R. J., Sugiyama, Y., Scholl, D. W., & Dinterman, P. A. (2003). Basin‒

696   centered asperities in great subduction zone earthquakes: A link between slip, subsidence,

697   and subduction erosion? *Journal of Geophysical Research,* 108, 2507.

698   https://doi.org/10.1029/2002JB002072

699 Wirth, E., Frankel, A., Marafi, N., Vidale, J., & Stephenson, W. (2018). Broadband synthetic

700   seismograms for magnitude 9 earthquakes on the Cascadia megathrust based on 3D

701   simulations and stochastic synthetics, Part 2: Rupture parameters and variability. Bulletin of

702   the Seismological Society of America, 108(5A), 2370– 2388.

703   https://doi.org/10.1785/0120180029

704 Xie, Z., & Cai, Y. (2018). Inverse method for static stress drop and application to the 2011

705   Mw9.0 Tohoku-Oki earthquake. *Journal of Geophysical Research: Solid Earth,* 123, 2871-

706   2884. https://doi.org/10.1002/2017JB014871

707 Yue, H., Lay, T., Rivera, L., An, C., Vigny, C., Tong, X., & Báez Soto, J. C. (2014). Localized

708   fault slip to the trench in the 2010 Maule, Chile Mw = 8.8 earthquake from joint inversion

709   of high‒rate GPS, teleseismic body waves, InSAR, campaign GPS, and tsunami

710   observations. *Journal of Geophysical Research: Solid Earth,* 119, 7786-7804.

711   https://doi.org/10.1002/2014JB011340